Regge phenomenology of the N^* and Δ^* poles

J. A. Silva-Castro,[1, *] C. Fernández-Ramírez,[1, †] M. Albaladejo,[2, 3] I. V. Danilkin,[4]
A. Jackura,[5, 6] V. Mathieu,[2] J. Nys,[7] A. Pilloni,[2] A. P. Szczepaniak,[2, 5, 6] and G. Fox[8]

(Joint Physics Analysis Center)

[1] *Instituto de Ciencias Nucleares, Universidad Nacional Autónoma de México, Ciudad de México 04510, Mexico*
[2] *Theory Center, Thomas Jefferson National Accelerator Facility, Newport News, VA 23606, USA*
[3] *Departamento de Física, Universidad de Murcia, E-30071 Murcia, Spain*
[4] *Institut für Kernphysik & PRISMA Cluster of Excellence, Johannes Gutenberg Universität, D-55099 Mainz, Germany*
[5] *Center for Exploration of Energy and Matter, Indiana University, Bloomington, IN 47403, USA*
[6] *Physics Department, Indiana University, Bloomington, IN 47405, USA*
[7] *Department of Physics and Astronomy, Ghent University, Belgium*
[8] *School of Informatics and Computing, Indiana University, Bloomington, IN 47405, USA*

We use Regge phenomenology to study the structure of the poles of the N^* and Δ^* spectrum. We employ the available pole extractions from partial wave analysis of meson scattering and photoproduction data. We assess the importance of the imaginary part of the poles (widths) to obtain a consistent determination of the parameters of the Regge trajectory. We compare the several pole extractions and we show how Regge phenomenology can be used to gain insight in the internal structure of baryons. We find that the majority of the states in the parent Regge trajectories are compatible with a mostly compact three-quark state picture.

I. INTRODUCTION

The baryon spectrum is one of the main tools for investigation of the nonperturbative QCD phenomena. In particular, the low-lying non-strange sector containing the N^* and Δ^* resonances, which is accessible in pion-nucleon scattering and photoproduction experiments, is a primary source of insights into the quark model. The goal of baryon spectroscopy is to understand the origin and structure of resonances, *e.g.* to establish if a given resonance can be classified as compact three quark ($3q$) state, as predicted by the quark model or that it has other hadronic components. This is often done through partial wave analyses, with resonances appearing in individual partial waves that are independently parametrized to fit the data. Such analyses miss global constraints imposed by the Regge theory that connect partial waves through analyticity in the angular momentum plane [1–3]. According to Regge theory, resonances appear as poles in the angular momentum plane. The pole location, which changes as a function of the resonance mass and defines the so-called Regge trajectory, can be used to study the microscopic mechanisms responsible for resonance formation [4–7].

The most noticeable feature of the hadron spectrum is that its Regge trajectories are approximately linear as shown by Chew and Frautschi [8]. The patterns implied by the Chew-Frautschi plot can be used to guide partial wave analyses. For example, gaps in the trajectories hint to missing states. The approximate linearity of Regge trajectories is one the strongest phenomenological indications of confinement [9] and therefore states belonging to linear trajectories are expected to be closely connected to quark model predictions [10, 11]. Resonance decays, modify trajectories and introduce imaginary parts. These are constrained by unitarity, analyticity and are related to resonance widths [12]. Consequently, Regge trajectories are a mapping of the complex energy plane, the s-plane, onto the complex angular momentum, the J plane. The linear curves that are shown on the Chew-Frautschi plots are the projections of the actual Regge trajectories onto the $(\Re[s], \Re[J])$ plane, and as such do not contain information about the imaginary part of the pole, *i.e.* the resonance width. In the past, resonance poles were often not computed and, with a few exceptions [13, 14], fits to the Chew-Frautschi plots gave the only information about the Regge trajectory. Constituent quark model predictions for hadron masses adhere nicely to the approximately linear behavior both in the baryon [15–22] and the meson [22–25] sectors. Flux tube models of baryons also provide linear trajectories [26–28].

In this article, following the analysis of the strange baryon sector [6] we use Regge phenomenology to study the N^* and Δ^* spectra. Resonance pole masses and widths are nowadays more prominently featured in the Particle Data Group (PDG) tables [29]. This is because, in the last years, amplitude analyses have become more sophisticated enabling for extraction of resonance poles from the experimental data. We fit complex Regge trajectories to the spectra obtained by several partial wave analyses [30–36] of meson scattering and photoproduction data. The objectives of this article are: (i) to provide a comprehensive comparison of the different N^* and Δ^* pole extractions based on Regge phenomenology; (ii) to assess the impact of neglecting the imaginary part of the poles in the computation of the Regge trajectory, in particular in the extraction of the slope parameter that can be compared to the one used in fits to the high energy

* jorge.silva@correo.nucleares.unam.mx
† cesar.fernandez@nucleares.unam.mx

proton-antiproton data [37]; and (iii) to guide future N^* and Δ^* pole extractions [38–40]. The paper is organized as follows. In Sec. II we review the N^* and Δ^* spectra available in the literature that will be used in our analysis. In Sec. III we describe the phenomenological models used to fit the spectrum and in Sec. IV we explain the fitting procedure, present the results and discuss the statistical analysis. Conclusions are given in Sec. V.

II. N^* AND Δ^* POLE EXTRACTIONS

For a given spin and parity, resonance pole positions s_p are extracted from partial wave amplitudes analytically continued off the real energy axis to the unphysical Riemann sheet. On the real axis the partial wave amplitudes are fitted to the data on meson-nucleon scattering and meson photoproduction. This procedure carries uncertainties associated to the experimental data (systematic and statistical), the partial wave analysis model itself, and the analytic continuation to the complex energy plane. The differences among models in the pole extractions reflect on some of these uncertainties and model dependencies. In Tables I-IV we list the poles that, in principle, conform the leading (parent), $i.e.$ the trajectory composed by the lowest mass states for each spin-parity assignment, N^* and Δ^* Regge trajectories, classified according to isospin I, naturality η ($\eta = +1$ if $P = (-1)^{J_p-1/2}$ and $\eta = -1$ if $P = -(-1)^{J_p-1/2}$ where P is the parity and J_p is the spin of the resonance), and signature τ ($\eta = \tau P$). The quantum numbers identify a given $I_{(\tau)}^{\eta}$ trajectory, $e.g.$ the trajectory which contains $N(939)$ (the nucleon) corresponds to $I_{(\tau)}^{\eta} = \frac{1}{2}\,^+_{(+)}$. Phenomenologically, it is observed that the leading Regge trajectories that differ only by signature are (almost) degenerate, $i.e.$ odd ($\tau = -$) and even ($\tau = +$) signatures have the same trajectory. For subleading trajectories there is often not enough information to disentangle both signatures. We use seven sets of resonance poles extracted from the following analyses:

(i) **CMB**: Pole parameters from the Carnegie-Mellon-Berkeley πN partial wave analysis of [30, 31] as quoted by the PDG [29];

(ii) **JüBo**: Pole parameters from [32] using the Jülich-Bonn 2017 coupled-channel model. The resonance spectrum is obtained from a combined analysis of η, π and $K\Lambda$ photoproduction off the proton together with the reactions $\pi N \to \pi N$, ηN, $K\Lambda$ and $K\Sigma$;

(iii) **BnGa**: Pole parameters given in [33, 34] from the Bonn-Gatchina multichannel partial wave analysis of πN elastic scattering data and pion and photo-induced inelastic reactions;

(iv) **SAID(SE)**: Pole parameters obtained in [35] from a fit to the single-energy SAID-GW WI08 partial waves of πN elastic scattering [41] using the Laurent+Pietarinen (LP) approach;

(v) **SAID(ED)**: Poles extracted in [35] from the energy-dependent SAID-GW WI08 partial waves of πN elastic scattering [41] also using the LP approach;

(vi) **KH80**: Pole extracted in [36] from the Karlsruhe-Helsinki KH80 [42] partial wave analysis of πN elastic scattering employing the LP approach; and

(vii) **KA84**: Pole extracted in [36] from the Karlsruhe KA84 [43, 44] partial wave analysis of πN elastic scattering employing the LP approach.

Other pole extractions are available in the literature. These include, the speed plot extraction from $\pi N \to \pi N$ amplitudes by Höhler [45]; the SAID pole parameters given in [35] obtained from the SAID-GW WI08 partial wave analysis of πN elastic scattering [41]; the Kent State University (KSU) pole extraction in [46] using a multichannel parametrization of πN scattering amplitudes; the Pittsburgh-Argonne National Lab (P-ANL) pole extraction in [47]; the Giessen group coupled-channel analysis of η production and photoproduction data on the proton [48]; the Argonne National Lab-Osaka (ANL-O) amplitude analysis of $\pi N \to \pi N$, ηN, $K\Lambda$, $K\Sigma$ and $\gamma N \to \pi N$, $\eta N, K\Lambda$, $K\Sigma$ data [49]; and the Zagreb analysis in [50] based on the CMB coupled-channel approach; Höhler, SAID, KSU, P-ANL, Giessen and ANL-O do not provide uncertainties in their pole extractions and the Zagreb group analysis only studies the N^* spectrum, hence, we choose not to include them in our work. Also, we do not include superseded pole extractions within the same reaction models.

In Fig. 1 we show the Chew-Frautschi plots $(\Re[s_p], \Re[J] = J_p)$ for the N^* and Δ^* resonances, and Fig. 2 displays the $(\Im[s_p], \Re[J] = J_p)$ plots introduced in [6]. These figures provide a qualitative description of the spectrum. We note the spectrum exhibits the approximate linear behavior in $(\Re[s_p], J_p)$ and the square root-like behavior in $(\Im[s_p], J_p)$. This was also observed in the spectrum of the hyperons [6]. We defer the discussion of the plots to Sec. IV, where we present the quantitative analysis of the spectrum.

III. MODELS FOR THE PARENT REGGE TRAJECTORIES

In what follows the working hypothesis is that the square-root-like behavior displayed in Fig. 2 is the leading singularity of the trajectories as implied by unitarity [51]. This stems from the fact that the leading two-body decay channels,$i.e.$ those that account for most of the cross section, give the imaginary part proportional to the relative momentum $q \sim \sqrt{s - s_t}$, where s is the two-body invariant mass squared and s_t is the threshold. Contribution from multi-body final states can effectively be absorbed

Table I. Summary of pole positions M_p, Γ_p in MeV for $I^\eta = \frac{1}{2}^+$ states where $M_p = \Re\sqrt{s_p}$ and $\Gamma_p = -2\Im\sqrt{s_p}$. I stands for isospin, η for naturality, J_p for spin, and P for parity. Naturality and parity are related by $\eta = \tau P$ where τ is the signature. For baryons, $\eta = +1$, natural parity, if $P = (-1)^{J_p - 1/2}$, and $\eta = -1$, unnatural parity, if $P = -(-1)^{J_p - 1/2}$.

Name	$N(939)$	$N(1520)$	$N(1680)$	$N(2190)$	$N(2220)$
Status	****	****	****	****	****
$I^\eta_{(\tau)} J^P_p$	$\frac{1}{2}^+_{(+)} 1/2^+$	$\frac{1}{2}^+_{(-)} 3/2^-$	$\frac{1}{2}^+_{(+)} 5/2^+$	$\frac{1}{2}^+_{(-)} 7/2^-$	$\frac{1}{2}^+_{(+)} 9/2^+$
CMB	939(1), 0	1510(5), 114(10)	1667(5), 110(10)	2100(50), 400(160)	2160(80), 480(100)
JüBo	939(1), 0	1509(5), 98(3)	1666(4), 81(2)	2084(7), 281(6)	2207(89), 659(140)
BnGa	939(1), 0	1507(3), 111(5)	1676(6), 113(4)	2150(25), 325(25)	2150(35), 440(40)
SAID(SE)	939(1), 0	1512(2), 113(6)	1678(4), 113(3)	2132(24), 550(25)	2173(7), 445(21)
SAID(ED)	939(1), 0	1515(2), 109(4)	1674(3), 114(7)	2060(11), 521(16)	2177(4), 464(9)
KH80	939(1), 0	1506(2), 115(3)	1674(3), 129(4)	—	2127(27), 380(29)
KA84	939(1), 0	1506(2), 116(4)	1672(3), 132(5)	—	2139(6), 390(7)

Table II. Summary of pole positions M_p, Γ_p in MeV for $I^\eta = \frac{1}{2}^-$ states. Notation as in Table I.

Name	$N(1720)$	$N(1675)$	$N(1990)$	$N(2250)$
Status	****	****	**	****
$I^\eta_{(\tau)} J^P_p$	$\frac{1}{2}^-_{(-)} 3/2^+$	$\frac{1}{2}^-_{(+)} 5/2^-$	$\frac{1}{2}^-_{(-)} 7/2^+$	$\frac{1}{2}^-_{(+)} 9/2^-$
CMB	1680(30), 120(40)	1660(10), 140(10)	1900(30), 260(60)	2150(50), 360(100)
JüBo	1689(4), 191(3)	1647(8), 135(9)	2152(12), 225(20)	1910(53), 243(73)
BnGa	1670(25), 430(100)	1655(4), 147(5)	1970(20), 250(20)	2195(45), 470(50)
SAID(SE)	1668(24), 303(58)	1661(1), 147(2.4)	2157(62), 261(104)	2283(10), 304(31)
SAID(ED)	1659(11), 303(19)	1657(3), 139(5)	—	2224(5), 417(10)
KH80	1677(5), 184(9)	1654(2), 125(4)	2079(13), 509(23)	2157(17), 412(51)
KA84	1685(5), 178(9)	1656(1), 123(3)	2065(14), 526(9)	2187(7), 396(25)

into model parameters. Near a Regge pole, partial wave amplitudes are proportional to

$$t_\ell(s) \propto \frac{1}{\ell - \alpha(s)}, \tag{1}$$

where $\alpha(s)$ is the Regge trajectory and ℓ is the total angular momentum of the partial wave. This can be compared to the Breit-Wigner amplitude close to the s_p pole under the approximation of elastic two-body scattering,[1]

$$t_\ell(s) \propto \frac{g^2}{M^2 - s - i g^2 \rho(s, s_t)}, \tag{2}$$

where M is real, sometimes referred to as the Breit-Wigner mass. Resonance decay is determined by g^2, which can be used to define coupling to open channels and $\rho(s, s_t)$ which is the phase space factor. With the determination of $\rho(s, s_t)$ that is analytical across the real axis for $s > s_t$ one finds poles of $t_\ell(s)$ located on the lower

---

[1] We note that both Eqs. (1) and (2) are written in the second Riemann sheet of the complex s plane, where the resonant poles in the amplitude appear.

half s-plane that are analytically connected to the physical region at $s + i\epsilon$. How deep a pole is in the complex plane depends on two factors, the dynamics of QCD and the phase space. The phase space dependence $\rho(s, s_t)$ is explicitly built in through unitarity and QCD dynamics are hidden in the parameters, M and g. At the pole s_p, Eqs. (1) and (2) have to be equal, hence

$$\ell - \alpha(s_p) = \frac{M^2}{g^2} - \frac{s_p}{g^2} - i\rho(s_p, s_t) = 0. \tag{3}$$

This equation is used to relate the imaginary part of the Regge trajectory to resonance decay parameters. Without loss of generality, we can parametrize the Regge trajectory as [6, 52, 53]

$$\alpha(s) = \alpha_0 + \alpha' s + i\,\gamma\,\phi(s, s_t), \tag{4}$$

where α_0, α' and γ are real constants, and $\phi(s, s_t)$ contains information about resonance decay. The slope α' is often related to the tension of the confining string in flux tube models [26–28] and to the range of the strong interaction in Veneziano models [54]. The square-root-like behavior in Fig. 2 hints that $\rho(s, s_t)$ is the dominant component of $\phi(s, s_t)$. Hence, as a first approximation, we can model $\gamma\phi(s, s_t) = \rho(s, s_t)$, and fit the trajectory

Table III. Summary of pole positions M_p, Γ_p in MeV for $I^\eta = \frac{3}{2}^+$ states. Notation as in Table I.

Name	$\Delta(1700)$	$\Delta(1905)$	$\Delta(2200)$	$\Delta(2300)$
Status	****	****	***	**
$I^\eta_{(\tau)} \, J^P_p$	$\frac{3}{2}^+_{(-)} \, 3/2^-$	$\frac{3}{2}^+_{(+)} \, 5/2^+$	$\frac{3}{2}^+_{(-)} \, 7/2^-$	$\frac{3}{2}^+_{(+)} \, 9/2^+$
CMB	1675(25), 220(40)	1830(40), 280(60)	2100(50), 340(80)	2370(80), 420(160)
JüBo	1667(28), 305(45)	1733(47), 435(264)	2290(132), 388(204)	—
BnGa	1685(10), 300(15)	1800(6), 290(15)	—	—
SAID(SE)	1646(11), 203(17)	1831(7), 329(17)	—	—
SAID(ED)	1652(10), 248(28)	1814(5), 273(9)	—	—
KH80	1643(9), 217(18)	1752(5), 346(8)	—	—
KA84	1616(5), 280(9)	1790(5), 293(12)	—	—

Table IV. Summary of pole positions M_p, Γ_p in MeV for $I^\eta = \frac{3}{2}^-$ states. Notation as in Table I.

Name	$\Delta(1232)$	$\Delta(1930)$	$\Delta(1950)$	—	$\Delta(2420)$
Status	****	***	****	—	****
$I^\eta_{(\tau)} \, J^P_p$	$\frac{3}{2}^-_{(-)} \, 3/2^+$	$\frac{3}{2}^-_{(+)} \, 5/2^-$	$\frac{3}{2}^-_{(-)} \, 7/2^+$	$\frac{3}{2}^-_{(+)} \, 9/2^-$	$\frac{3}{2}^-_{(-)} \, 11/2^+$
CMB	1210(1), 100(2)	1890(50), 260(60)	1890(15), 260(40)	—	2360(100), 420(100)
JüBo	1215(4), 97(2)	1663(43), 263(76)	1850(37), 259(61)	1783(86), 244(194)	—
BnGa	1210.5(1.0), 99(2)	—	1888(4), 245(8)	—	—
SAID(SE)	1211(0), 100(2)	1845(31), 174(40)	1888(3), 234(6)	—	—
SAID(ED)	1211(2), 98(3)	1969(23), 248(36)	1878(4), 227(6)	1955(24), 911(24)	2320(13), 442(23)
KH80	1211(2), 98(3)	1848(28), 321(24)	1877(3), 223(5)	—	2454(15), 462(58)
KA84	1210(2), 100(2)	1844(36), 334(26)	1878(3), 246(7)	—	2301(7), 533(17)

in Eq. (4) at the poles $s = s_p$ to $\Re[\alpha(s_p)] = \Re[J] = J_p$ and $\Im[\alpha(s_p)] = \Im[J] = \Im[J_p] = 0$ obtaining α_0, α', γ and s_t. The parameter α_0 is dimensionless, the slope α' has units of GeV^{-2}, s_t acts as an effective threshold that has units of GeV^2. The systematic uncertainties of the model associated with the description of the phase space factor far away from the threshold can be studied by considering different models for $\phi(s, s_t)$. In particular we use,

$$i\,\phi_0(s, s_t) = 0, \tag{5a}$$

$$i\,\phi_\mathrm{I}(s, s_t) = i\sqrt{s - s_t}, \tag{5b}$$

$$i\,\phi_\mathrm{II}(s, s_t) = \beta(s, s_t) + 2i\tau(s, s_t), \tag{5c}$$

where

$$
\begin{aligned}
i\beta(s, s_t) &= \frac{s - s_t}{\pi} \int_{s_t}^\infty \frac{\tau(s', s_t)}{s' - s_t} \frac{ds'}{s' - s} \\
&= \frac{2}{\pi} \frac{s - s_t}{\sqrt{s(s_t - s)}} \arctan\sqrt{\frac{s}{s_t - s}}\,, \tag{6}
\end{aligned}
$$

is the analytic continuation of the two-body phase space[2] $\tau(s, s_t) = \sqrt{1 - s_t/s}$ to the complex s plane. It follows that in Eq. (4), γ has units of GeV^{-1} for model I and is dimensionless in model II. Model 0 is the customary linear dependency that ignores the existence of the imaginary part of the resonance poles. Although essential physics is ignored in such model, we fit it to $\Re[s_p]$ for completeness and to provide a comparison to previous works. We note that once the width of the resonance pole is taken into account it is clear that a Regge trajectory cannot be linear. Linear Regge trajectories can only happen for zero-width resonances, e.g. resonances computed as bound states in a constituent quark model, or the tower of states in the Veneziano amplitude [55]. Models I and II do incorporate such physics by adding an imaginary part to $\alpha(s)$ in a simple way. Model I is a customary approach to add the imaginary part to $\alpha(s)$ which has been used to account for unitarity effects in Veneziano-type amplitudes [56–58]. Model II is the most physically motivated as it is guided by the relation between Eqs. (1) and (2), $\beta(s, s_t)$ is the analytic continuation of the phase space,

---

[2] We assume elastic two-body scattering, and hence, all poles are considered to be in the second Riemann sheet. That is also the reason why we fit an effective threshold s_t instead of using the actual physical thresholds.
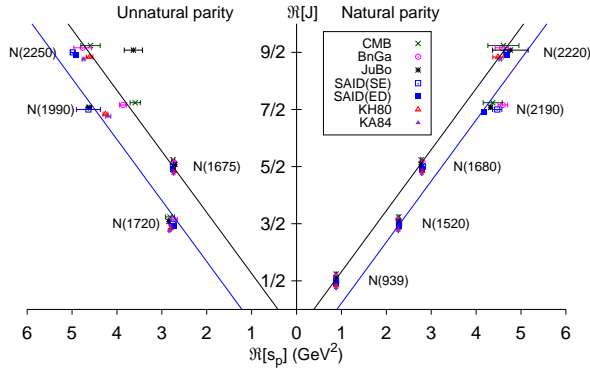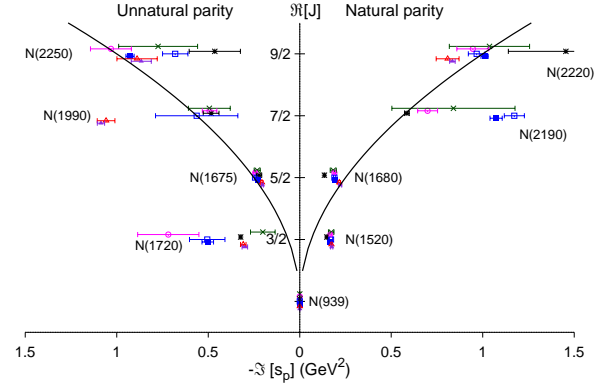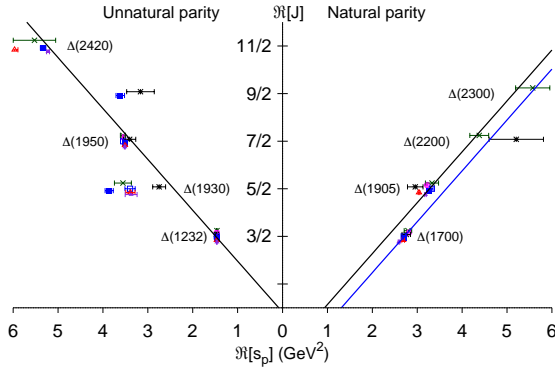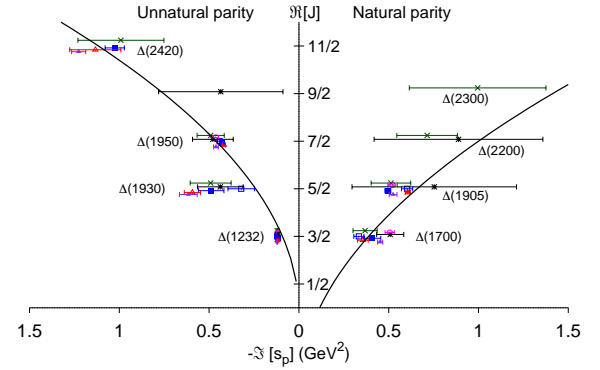
(a) N^* resonances.

(a) N^* resonances.

(b) Δ^* resonances.

(b) Δ^* resonances.

Figure 1. Chew–Frautschi plots for the leading N^* and Δ^* Regge trajectories in Tables I-IV. Solid black (blue) lines guide the eye through the $\tau = +$ ($\tau = -$) trajectories (see Sec. IV B for details). All the lines share the same slope. In order to make the plots readable, the poles are slightly displaced from the correct $\Re[J] = J_p$ value.

Figure 2. $(\Im[s_p], \Re[J] = J_p)$ plots introduced in [6] for the leading N^* and Δ^* Regge trajectories in Tables I-IV. Lines are displayed to guide the eye. The different pole sets are labeled as in Fig. 1. In order to make the plots readable, the poles are slightly displaced from the correct $\Re[J] = J_p$ value as in Fig. 1. SAID(ED) Δ $9/2^-$ pole in the unnatural parity trajectory has a very large $\Im[s_p]$ value and it is not shown in plot (b).

Chew-Mandelstam dispersive approach [51], and $\phi(s, s_t)$ is the analytic continuation of $\beta(s, s_t)$ to the second Riemann sheet, as dictated by unitarity. However, we will compute the three models for the sake of completeness and comparison purposes.

Our hypothesis to interpret the nature of the resonances in terms of the Regge trajectory is that a state that is located on a linear trajectory in the Chew-Frautschi plot *and* a square-root-like behavior in $(\Im[s_p], J_p)$ plot would be mostly a compact $3q$ state. Hence, most of the width, *i.e.* the contribution to $\phi(s, s_t)$, would be due to the phase space. If it is so, the poles should adhere nicely to our Regge trajectory mod-

els. If the resonance pole is not well described by our models, it is an indication that additional QCD dynamics are important, signaling that the state has significant physics beyond the compact $3q$ picture.

IV. RESULTS

A. Fits and error analysis

To determine the parameters α_0, α', γ and s_t in Eq. (4) for a given pole extraction we use the least-squares method by minimizing the distance squared d^2 between the trajectory $\alpha(s)$ evaluated at the complex pole position s_p and the angular momenta J,

$$d^2 = \sum_{poles} \left\{ \left[\Re[J] - \Re[\alpha(s_p)] \right]^2 + \left[\Im[J] - \Im[\alpha(s_p)] \right]^2 \right\}.$$

with $\Re[J] = J_p$ and $\Im[J] = \Im[J_p] = 0$ for the resonance poles. The value of s_t should be compatible with its interpretation as an effective threshold in the resonance region. This is used as the criterion to select the physically meaningful minimum if several local minima appear in the fits. We estimate the errors in the parameters through the bootstrap technique [59–61]. In doing so, we perform 10^4 fits to pseudodata generated according to the pole uncertainties. The expected value of each parameter is computed as the mean of the 10^4 samples and the uncertainty is given by the standard deviation. This method is described in detail in [6, 62] and allows to propagate the uncertainties from the poles to the parameters accounting for all the correlations. The systematic errors associated with model dependence in the amplitude analyses are not considered in the pole extractions, hence, we take the differences among models as an indication of such uncertainties. The fit results are provided and discussed in Sec. IV B. As an additional test of our results we perform consistency checks as described in [6]. Specifically, once we have the fit parameters we can use them to compute the value of the Regge trajectory at the pole positions, hence, for a resonance with pole position s_p and spin J_p we should recover $\Re[\alpha(s_p)] = \Re[J] = J_p$ and $\Im[\alpha(s_p)] = \Im[J] = \Im[J_p] = 0$. The latter condition is particularly stringent. Consistency checks for trajectories with only two poles do not provide any information because they are overfitted, (four experimental points, two masses and two widths, fitted with four parameters). Hence we only compute the consistency checks for trajectories with more than two poles. The uncertainties in the poles and the parameters are propagated to the calculation of $\alpha(s)$.

B. Regge trajectories

1. $\frac{1}{2}^+$ Regge trajectory

In Regge analyses of the hadron spectrum it is customary to consider as the $I^\eta = \frac{1}{2}^+$ parent trajectory the one containing the states in Table I and higher spins if available. This trajectory contains two nearly degenerate Regge trajectories corresponding to odd and even signatures. The degeneracy appears when the exchange forces

Table V. Parameter α_0 obtained for $\frac{1}{2}^+$ trajectories and models 0, I and II.

$I^\eta_{(\tau)}$	Pole set	$\alpha_0^{(0)}$	$\alpha_0^{(I)}$	$\alpha_0^{(II)}$
$\frac{1}{2}^+_{(+)}$	CMB	$-0.4(1)$	$0.3(2)$	$0.3(3)$
	JüBo	$-0.3(1)$	$0.6(1)$	$0.9(3)$
	BnGa	$-0.46(5)$	$0.20(7)$	$0.1(2)$
	SAID(SE)	$-0.42(1)$	$0.25(3)$	$0.22(6)$
	SAID(ED)	$-0.41(1)$	$0.29(2)$	$0.30(3)$
	KH80	$-0.50(4)$	$-0.1(2)$	$-0.2(1)$
	KA84	$-0.48(1)$	$0.05(3)$	$-0.09(3)$
$\frac{1}{2}^+_{(-)}$	CMB	$-0.6(1)$	$-0.8(3)$	$-3.5(7)$
	JüBo	$-0.71(3)$	$-0.79(4)$	$-1.53(6)$
	BnGa	$-0.44(7)$	$-0.53(7)$	$-1.5(5)$
	SAID(SE)	$-0.53(7)$	$-0.9(1)$	$-4.6(3)$
	SAID(ED)	$-0.86(4)$	$-1.25(6)$	$-5.54(3)$

Table VI. Parameter α' obtained for $\frac{1}{2}^+$ trajectories.

$I^\eta_{(\tau)}$	Pole set	$\alpha'^{(0)}$	$\alpha'^{(I)}$	$\alpha'^{(II)}$
$\frac{1}{2}^+_{(+)}$	CMB	$1.06(7)$	$0.85(6)$	$0.9(1)$
	JüBo	$1.00(8)$	$0.72(6)$	$0.8(1)$
	BnGa	$1.07(3)$	$0.87(3)$	$1.04(6)$
	SAID(SE)	$1.04(1)$	$0.85(1)$	$0.99(1)$
	SAID(ED)	$1.036(4)$	$0.84(1)$	$0.97(1)$
	KH80	$1.10(2)$	$0.98(6)$	$1.14(5)$
	KA84	$1.08(1)$	$0.93(1)$	$1.10(1)$
$\frac{1}{2}^+_{(-)}$	CMB	$0.94(7)$	$0.95(9)$	$1.6(2)$
	JüBo	$0.97(1)$	$0.98(1)$	$1.23(2)$
	BnGa	$0.85(3)$	$0.86(3)$	$1.15(6)$
	SAID(SE)	$0.89(3)$	$0.92(3)$	$2.0(1)$
	SAID(ED)	$1.03(2)$	$1.06(2)$	$2.27(2)$

Table VII. Parameters γ and s_t obtained for $\frac{1}{2}^+$ trajectories.

$I^\eta_{(\tau)}$	Pole set	$\gamma^{(I)}$	$\gamma^{(II)}$	$s_t^{(I)}$	$s_t^{(II)}$
$\frac{1}{2}^+_{(+)}$	CMB	$0.49(7)$	$0.66(7)$	$2.4(2)$	$1.04(9)$
	JüBo	$0.62(8)$	$0.67(5)$	$2.65(5)$	$1.3(1)$
	BnGa	$0.46(3)$	$0.65(4)$	$2.4(1)$	$0.96(3)$
	SAID(SE)	$0.46(2)$	$0.64(2)$	$2.44(3)$	$0.98(1)$
	SAID(ED)	$0.48(1)$	$0.65(1)$	$2.46(3)$	$1.00(1)$
	KH80	$0.39(3)$	$0.65(3)$	$1.8(4)$	$0.91(1)$
	KA84	$0.41(1)$	$0.64(1)$	$2.06(7)$	$0.92(1)$
$\frac{1}{2}^+_{(-)}$	CMB	$0.5(2)$	$1.9(5)$	$2.3(4)$	$2.9(6)$
	JüBo	$0.39(1)$	$0.95(3)$	$2.17(2)$	$2.34(1)$
	BnGa	$0.38(3)$	$1.0(1)$	$2.17(3)$	$2.42(4)$
	SAID(SE)	$0.72(5)$	$3.0(2)$	$2.39(2)$	$2.79(2)$
	SAID(ED)	$0.82(3)$	$3.15(5)$	$2.40(1)$	$2.78(3)$

are weak and, then, both trajectories overlap [1]. This was the case for both Λ and Σ trajectories in [6] but it is not the case for the $\frac{1}{2}^+$ states as it is apparent in Fig. 1(a), where the degeneracy is broken and signature $\tau = +$ (the nucleon trajectory with $N(939)$, $N(1680)$, and $N(2220)$ states) and $\tau = -$ ($N(1520)$ and $N(2190)$ states) trajectories have different parameters. In particular, from Fig. 1(a) it is apparent that α_0 has to be different for each signature. Hence, we treat both trajectories separately. We expect both fits to share approximately the same slope parameter α' [1] and a different α_0 that encodes information on the breaking of the degeneracy, *i.e.* on the exchange forces.

The inspection of the natural parity poles in Figs. 1(a) and 2(a) highlights the agreements and disagreements among the pole extractions. All the extractions reasonably agree for $\Re[s_p]$ for all the states poles but either disagree or have very large uncertainties for $N(2190)$ and $N(2220)$ widths. We note how BnGa and SAID(SE) extractions of $N(2190)$ separate from the expected straight line depicted in Fig. 1(a). This is interesting because $I^\eta_{(\tau)} = \frac{1}{2}^+_{(+)}$ and $\frac{1}{2}^+_{(-)}$ trajectories are expected to have the same slope α' [1], and the position of $N(2190)$ for both extractions is at odds with this expectation. Considering both Figs. 1(a) and 2(a), only JüBo and CMB provide a $N(2190)$ extraction that conforms to the expected position of the pole within uncertainties, although the CMB error is very large. For $N(2220)$ all the analyses coincide on $\Re[s_p]$ but differ wildly regarding the width.[3]

Figure 3 shows the consistency checks for $\frac{1}{2}^+_{(-)}$ for CMB, JüBo, BnGa and SAID(ED) which provide a sharper comparison. The consistency checks for SAID(SE), KH80 and KA84 are redundant and we do not show them. The $\frac{1}{2}^+_{(-)}$ consistency checks are not shown because they are overfitted and do not provide any information. The $\frac{1}{2}^+_{(+)}$ does provide insight, showing how the poles deviate from the proposed model. If we ignore model 0, which misses the resonant physics, the nondispersive model (I) provides, on average, a better consistency check than the dispersive one (II) for all the extractions. However, this better description of $N(1680)\,J_p^P = 5/2^+$ and $N(2220)\,9/2^+$ states is achieved by spoiling the agreement with the nucleon $N(939)\,1/2^+$. These are clear indications that there is tension between the states and our trajectory parametrization. The $N(2220)$ has large uncertainties for all the extractions and its weight on the determination of the Regge trajectory is smaller than the nucleon and the $N(1680)$ states, which have small errors. Besides, all the extractions agree fairly well regarding the pole position of the $N(1680)$.
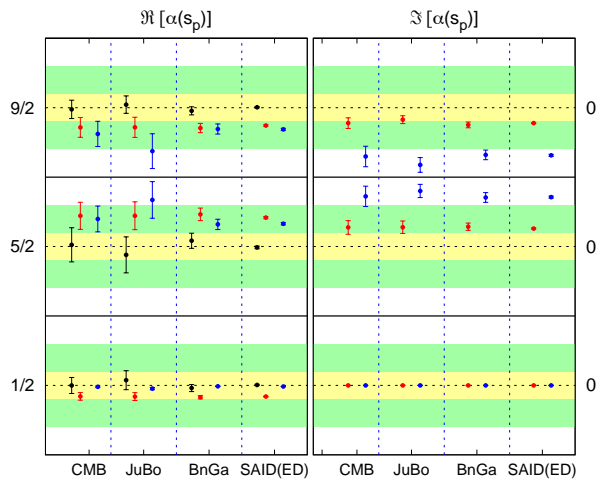
---

[3] We remind the reader that the deeper in the complex plane the pole is, the larger the systematic uncertainties associated to the models and to the analytic continuation into the unphysical Riemann sheets.

Figure 3. Consistency checks (see Sec. IV A) for $I^\eta_{(\tau)} = \frac{1}{2}^+_{(+)}$ poles from CMB, JüBo, BnGa, and SAID(ED) extractions. The left plot shows $\Re[\alpha(s_p)]$ (see Table I and Sec. IV B 1 for their definition), computed at the poles of the resonances (s_p) for models 0 (black), I (red) and II (blue). The result should be equal to the corresponding angular momentum $\Re[J] = J_p$ (vertical axis) for a given resonance. The right plots depict the same calculation for $\Im[\alpha(s_p)]$, which should be equal to $\Im[J] = \Im[J_p] = 0$. In this latter case we do not show model 0 because $\Im[\alpha(s_p)] = 0$ by definition. The yellow (green) bands represent up to 0.1 (from 0.1 to 0.3) deviation from the label in the vertical axis. The white band represents from 0.3 to 0.5 deviation.

Hence, there is a strong indication that the approximation of $\gamma\phi(s, s_t) = \rho(s, s_t)$ is not valid for the $N(1680)$, signaling a sizeable contribution from physics beyond the compact $3q$ picture. We note that constituent quark models have problems reproducing the mass of this state and they usually overestimate it [17, 19, 20].

These differences are more apparent if we compare the fits to the pole sets with the three models. We provide the fit parameters in Tables V–VII. First, the value of s_t represents an effective threshold for the phase space and its fitted value should be consistent with such interpretation, *i.e.* $s_t \sim (m_\pi + m_N)^2 \simeq 1.17\,\text{GeV}^2$. This is used as a criterion to select the physically meaningful minimum if several local minima appear in the fits, and to partly assess the quality of the Regge parameters. For the $\frac{1}{2}^+_{(+)}$ trajectory, all s_t in Table VII are reasonable for model II (between 0.92 and 1.3 GeV^2) while they are larger for model I (between 1.8 and 2.65 GeV^2). This asserts the better physical motivation of model II compared to model I. Therefore, we consider the parameters provided by model II as more reliable. For $\frac{1}{2}^+_{(-)}$ we only have two states to estimate the trajectory parameters, however it is enough to test, together with the information on $\frac{1}{2}^+_{(+)}$, how well the states conform to the $\gamma\phi(s, s_t) = \rho(s, s_t)$ hypothesis. Both models provide a large value for s_t ranging from 2.17 to 2.9, hence the slope extraction is

Table VIII. $\Delta\alpha_0 \equiv \alpha_0(\tau = +) - \alpha_0(\tau = +)$ for the $\frac{1}{2}^+$ trajectories and the three models. Uncertainties obtained adding errors in quadrature.

Pole set	Model 0	Model I	Model II
CMB	0.2(1)	1.1(4)	3.8(8)
JüBo	0.4(1)	1.4(1)	2.4(3)
BnGa	−0.02(9)	0.7(1)	1.6(5)
SAID(SE)	0.11(7)	1.2(1)	4.8(3)
SAID(ED)	0.45(4)	1.54(6)	5.84(7)

not as reliable as for the $\frac{1}{2}^+_{(+)}$ trajectory.

The slope parameter α' links low-lying resonances and high-energy scattering physics, $e.g.$ nucleon-antinucleon annihilation, as it drives the Reggeon exchange amplitude under the single pole exchange approximation [1]. Its value is usually taken from linear fits to the Chew-Frautschi plot using model 0 or estimated from proton-antiproton scattering as $\alpha' \simeq 0.98\,\text{GeV}^{-2}$ [37]. For $\frac{1}{2}^+_{(+)}$ we find that the α' extraction is very consistent across the pole extractions. Restricting ourselves to model II, we can estimate the slope as

$$\alpha'_{\frac{1}{2}^+_{(+)}} = 0.99 \pm 0.12\,\text{GeV}^{-2},$$

where the best value and the uncertainty have been computed averaging through a bootstrap the seven α' in Table VI. These values are not very different from the ones obtained with model 0, $\alpha'^{(0)} \simeq 1\,\text{GeV}^{-2}$, and neglecting the widths does not have a large impact in α'. These results are also in agreement with what is expected from algebraic [17, 18] ($\alpha' = 1.07 \pm 0.02\,\text{GeV}^{-2}$) and relativistic [20] ($\alpha' \simeq 1\,\text{GeV}^{-2}$) quark models, despite the fact that they miss dynamics [63] that are present in the actual Regge trajectories. The $\frac{1}{2}^\pm$ trajectories should have the same slope [1], hence once we have a robust determination from the $\frac{1}{2}^+_{(+)}$ we can use it to benchmark and assess the parameters extracted from other trajectories.

Regarding the $\frac{1}{2}^+_{(-)}$ slope, all pole extractions agree for model I and are consistent with $\frac{1}{2}^+_{(+)}$. However, we find large differences for model II. The only extractions that provide a consistent picture throughout the three models of the trajectory are BnGa and JüBo, $i.e.$ $\sqrt{s_t} \simeq 1.45 - 1.55$ GeV is closer to the expected value of $\sqrt{s_t} \sim m_\pi + m_p \simeq 1.08$ GeV than the other pole sets and $\alpha' \sim 1\,\text{GeV}^{-2}$ close to the extracted value from $\frac{1}{2}^+_{(+)}$ trajectory. Although JüBo has model II slope slightly larger than expected. The $N(1520)$ state is very well established and all the pole extractions agree. Hence, a better knowledge of this trajectory and an assessment on the nature of its states based on Regge phenomenology requires a better determination of the $N(2190)$ state and the $N\,11/2^-$ state.

As expected, α_0 is different for the two signatures (Table V). Considering $\frac{1}{2}^+_{(+)}$, the values of α_0 are very similar for models I and II across the different pole sets and different from model 0. Here we appreciate the impact in the trajectory parameter extraction due to the inclusion of the resonant nature of the states. However, the values of α_0 for $\frac{1}{2}^+_{(-)}$ change a lot from model to model and from pole extraction to pole extraction. This is mostly due to the discrepancies among models in the extraction of the width of $N(2190)$. In Table VIII we provide the difference $\Delta\alpha_0 = \alpha_0(\tau = +) - \alpha_0(\tau = -)$, for each model and pole extraction as a way to quantify the degeneracy breaking. The fact that each amplitude analysis provides a different value for $\Delta\alpha_0$ shows that the strength of the exchange forces are different among them. These forces are related to the left-hand cut of the amplitudes and are not well known. Hence, the range of values for $\Delta\alpha_0$ quantifies the magnitude of the uncertainties associated to this particular model dependency. Inspecting Table VIII it is noticeable that $\Delta\alpha_0$ for BnGa and model 0 is negative. This is related to the difference in the extraction of the slope parameter α' (1.07(3) and 0.85(3) in Table VI). However, if we introduce the widths in the analysis, $\Delta\alpha_0$ becomes positive (as expected from Fig. 1(a)) and the slopes become compatible within errors (0.87(3) and 0.86(3) for model I and 1.04(6) and 1.15(6) for model II). This again shows the importance of including the width in the analysis, and, moreover, how its inclusion leads to a better and more consistent estimation of both α_0 and the slope parameter α'. Our best estimation of α_0, using the same technique as for α' and model II, is

$$\alpha_{0,\frac{1}{2}^+_{(+)}} = 0.21 \pm 0.38.$$

The two remaining parameters are

$$\gamma_{\frac{1}{2}^+_{(+)}} = 0.651 \pm 0.040; \quad s_{t,\frac{1}{2}^+_{(+)}} = 1.02 \pm 0.13\,\text{GeV}^2,$$

with the effective threshold close to the expected value of $(m_\pi + m_p)^2 \simeq 1.17$ GeV^2.

2. $\frac{1}{2}^-$ Regge trajectory

In Table II we provide the lowest-lying states for each spin J_p compatible with the $\frac{1}{2}^-$ Regge trajectory except for the $N(1535)$ ($J_p^P = 1/2^-$) which belongs to a daughter trajectory. As for $\frac{1}{2}^+$ trajectory, we have two nearly degenerate trajectories with opposite signatures. However, the $(\Im[s_p], J_p)$ plot in Fig. 2(a) provides conflicting information about the $N(1720)\,3/2^+$ state. The large widths obtained by BnGa, SAID(SE) and SAID(ED), $\Gamma_p \sim 300 - 430$ MeV, would place this state in the daughter trajectory. However, CMB is compatible with $N(1720)$ ($\Gamma_p = 120$ MeV) belonging to the parent trajectory, and JüBo, KH80, and KA84 ($\Gamma_p \sim 185$ MeV) are in between both possibilities. If we look into the

Table IX. Parameter α_0 obtained for $\frac{1}{2}^-$ trajectories.

$I^\eta_{(\tau)}$	Pole set	$\alpha_0^{(0)}$	$\alpha_0^{(I)}$	$\alpha_0^{(II)}$
$\frac{1}{2}^-_{(+)}$	CMB	$-0.4(3)$	$-0.7(3)$	$-3(2)$
	JüBo	$-4(1)$	$-4(1)$	$-7(3)$
	BnGa	$-0.1(2)$	$-0.5(2)$	$-6(1)$
	SAID(SE)	$0.25(3)$	$0.16(4)$	$-0.5(2)$
	SAID(ED)	$0.01(3)$	$-0.21(3)$	$-2.3(1)$
	KH80	$-0.4(1)$	$-0.6(1)$	$-4(1)$
	KA84	$-0.19(3)$	$-0.41(5)$	$-3.0(5)$
$\frac{1}{2}^-_{(-)}$	CMB	$-6(1)$	$-6(2)$	$-9(2)$
	JüBo	$-1.7(1)$	$-1.8(1)$	$-2.1(1)$
	BnGa	$-3.6(5)$	$-3.0(6)$	$-3.0(6)$
	SAID(SE)	$-1.5(4)$	$-1.5(4)$	$-0.38(3)$
	KH80	$-2.2(1)$	$-2.9(2)$	$-10.2(4)$
	KA84	$-2.5(1)$	$-3.2(2)$	$-11.2(4)$

Table XI. Parameters γ and s_t obtained for $\frac{1}{2}^-$ trajectories.

$I^\eta_{(\tau)}$	Pole set	$\gamma^{(I)}$	$\gamma^{(II)}$	$s_t^{(I)}$	$s_t^{(II)}$
$\frac{1}{2}^-_{(+)}$	CMB	$0.6(2)$	$3(1)$	$2.6(2)$	$3.0(3)$
	JüBo	$1.0(4)$	$2(1)$	$2.2(5)$	$2.5(4)$
	BnGa	$0.70(9)$	$3.2(4)$	$2.73(4)$	$3.4(1)$
	SAID(SE)	$0.34(3)$	$0.9(1)$	$2.44(7)$	$2.7(1)$
	SAID(ED)	$0.56(1)$	$1.84(5)$	$2.69(2)$	$3.07(2)$
	KH80	$0.67(8)$	$1.14(5)$	$2.72(4)$	$3.1(1)$
	KA84	$0.59(3)$	$1.8(2)$	$2.71(2)$	$3.0(1)$
$\frac{1}{2}^-_{(-)}$	CMB	$1.4(5)$	$3(1)$	$2.6(4)$	$2.7(3)$
	JüBo	$0.31(4)$	$0.8(1)$	$1.3(4)$	$2.3(1)$
	BnGa	$0.6(1)$	$1.3(1)$	$1.02(4)$	$1.1(1)$
	SAID(SE)	$0.3(1)$	$0.63(2)$	$0.8(1)$	$1.52(1)$
	KH80	$1.2(1)$	$5.0(2)$	$2.84(3)$	$3.31(3)$
	KA84	$1.3(1)$	$5.5(2)$	$2.92(2)$	$3.31(2)$

Table X. Parameter α' obtained for $\frac{1}{2}^-$ trajectories.

$I^\eta_{(\tau)}$	Pole set	$\alpha'^{(0)}$	$\alpha'^{(I)}$	$\alpha'^{(II)}$
$\frac{1}{2}^-_{(+)}$	CMB	$1.1(1)$	$1.1(1)$	$1.8(5)$
	JüBo	$2.3(5)$	$2.3(5)$	$3(1)$
	BnGa	$0.97(7)$	$0.99(7)$	$2.1(2)$
	SAID(SE)	$0.81(1)$	$0.82(1)$	$1.03(4)$
	SAID(ED)	$0.91(1)$	$0.93(1)$	$1.46(2)$
	KH80	$1.04(3)$	$1.07(4)$	$1.8(2)$
	KA84	$0.98(1)$	$0.99(1)$	$1.6(1)$
$\frac{1}{2}^-_{(-)}$	CMB	$2.6(4)$	$2.6(4)$	$3.4(5)$
	JüBo	$1.13(3)$	$1.13(3)$	$1.28(4)$
	BnGa	$1.8(2)$	$1.6(2)$	$1.9(2)$
	SAID(SE)	$1.1(1)$	$1.1(1)$	$1.18(1)$
	KH80	$1.32(4)$	$1.37(4)$	$3.2(1)$
	KA84	$1.40(5)$	$1.50(5)$	$3.5(1)$

other pole extractions that we do not consider in our analysis, we see that SAID obtains 334 MeV [35], similar to BnGa, SAID(SE) and SAID(ED). Other pole sets are closer to the JüBo, KH80 and KA84 extractions, *e.g.* Höhler 187 MeV [45], KSU 175 MeV [46], and Zagreb 233 MeV [50]; while others obtain smaller widths compatible with the CMB result *e.g.* P-ANL 94 MeV [47], Giessen 118 MeV [48], and ANL-O 70 MeV [49]. We note that the discrepancies among pole extractions, together with constituent quark models predicting several $3/2^+$ states in the $N(1720)$ energy range [16, 17, 19, 20] make possible that what the different amplitude analysis are reporting is not just one resonant state but an effective pole that accounts for a more complicated picture. Moreover, the recent ANL-O pole extraction finds two states with masses 1703 and 1763 MeV and widths 70 and 159 MeV respectively [49]. Further research on this

energy range is necessary to establish mass and width of the state(s) with precision before discussing its (their) nature. In what follows, we include $N(1720)$ in our calculations as a member of the parent $\frac{1}{2}^-_{(-)}$ trajectory.

Contrary to $\frac{1}{2}^+$ resonances, $\frac{1}{2}^-$ states that belong to the leading Regge trajectory are not that well known, what predates any conclusion on the internal structure of the states that we can derive from fits. At this stage, Regge phenomenology can be used more effectively as a guide to improve amplitude analyses and pole extraction than to elucidate the nature of the resonances.

Figures 1 and 2 make apparent how different are the poles from one extraction to another. There is consensus only on the $N(1675)\,5/2^-$ state. This is a direct challenge to the four-star status of $N(1720)$ and $N(2250)$ resonances in the PDG [29]. We fit two trajectories $\frac{1}{2}^-_{(+)}$ ($N(1675)$ and $N(2250)$ states) and $\frac{1}{2}^-_{(-)}$ ($N(1720)$ and $N(1990)$ states). The obtained fit parameters are provided in Tables IX–XI. For the $\frac{1}{2}^-_{(+)}$, none of the pole extractions provides a good result for s_t. Besides, MacDowell symmetry [1, 64] imposes that the slopes for $\frac{1}{2}^+_{(+)}$ and $\frac{1}{2}^-_{(-)}$ ($\frac{1}{2}^+_{(-)}$ and $\frac{1}{2}^-_{(+)}$) should be equal. Hence, we should obtain $\alpha' \sim 1$ GeV^{-2} to agree with the results in Sec. IV B 1, a condition only SAID(SE) fulfills for the three models, despite the fact that its $s_t = 2.7$ GeV^2 is larger than expected. Regarding negative signature, only BnGa and SAID(ED) are close to $s_t \sim 1.2$ GeV^2. If we also consider the expected slope, the only pole extraction that provides reasonable parameters is SAID(ED). Finally, JüBo provides a higher $s_t = 2.3$ and a slightly large but reasonable slope. We do not provide plots with the consistency check as both trajectories are overfitted.

In summary, none of the pole sets provides a convincing picture of the $\frac{1}{2}^-$ trajectory and there is a reasonable pos-

Table XII. Parameter α_0 obtained for $\frac{3}{2}^+$ trajectory.

$I^{\eta}_{(\tau)}$	Pole set	$\alpha_0^{(0)}$	$\alpha_0^{(I)}$	$\alpha_0^{(II)}$
$\frac{3}{2}^+$	CMB	$-1.2(4)$	$-1.3(4)$	$-1.6(6)$
	JüBo	$-1.3(2)$	$-1.0(2)$	$-1.0(3)$
	BnGa	$-5.7(6)$	$-5.7(6)$	$-6.0(8)$
	SAID(SE)	$-2.7(3)$	$-3.2(3)$	$-7(1)$
	SAID(ED)	$-3.4(3)$	$-3.5(3)$	$-4.5(6)$
	KH80	$-5.9(6)$	$-7.2(8)$	$-22.7(2)$
	KA84	$-2.9(2)$	$-3.0(2)$	$-3.5(1)$
$\frac{3}{2}^+_{(+)}$	CMB	$-0.5(5)$	$-0.5(4)$	$-1.2(6)$
$\frac{3}{2}^+_{(-)}$	CMB	$-2.1(4)$	$-2.2(5)$	$-4(1)$
	Jübo	$1.0(7)$	$-1.2(6)$	$-1.8(9)$

Table XIV. Parameters γ and s_t obtained for $\frac{3}{2}^+$ trajectory.

$I^{\eta}_{(\tau)}$	Pole set	$\gamma^{(I)}$	$\gamma^{(II)}$	$s_t^{(I)}$	$s_t^{(II)}$
$\frac{3}{2}^+$	CMB	$0.5(1)$	$1.2(3)$	$2.0(6)$	$2.3(4)$
	JüBo	$0.5(2)$	$1.1(3)$	$2.0(2)$	$2.5(4)$
	BnGa	$0.9(1)$	$1.8(3)$	$0.9(2)$	$1.4(5)$
	SAID(SE)	$1.0(1)$	$3.0(5)$	$2.5(1)$	$2.8(1)$
	SAID(ED)	$0.7(1)$	$1.6(3)$	$1.3(7)$	$2.1(4)$
	KH80	$2.4(3)$	$9.4(1)$	$2.7(1)$	$2.94(2)$
	KA84	$0.6(1)$	$1.4(1)$	$0.8(5)$	$1.8(2)$
$\frac{3}{2}^+_{(+)}$	CMB	$0.4(1)$	$1.3(4)$	$1.7(5)$	$2.7(4)$
$\frac{3}{2}^+_{(-)}$	CMB	$0.6(2)$	$2.0(1)$	$1.9(6)$	$2.7(3)$
	Jübo	$0.6(3)$	$1.3(6)$	$2.5(1)$	$2.5(3)$

Table XIII. Parameter α' obtained for $\frac{3}{2}^+$ trajectory.

$I^{\eta}_{(\tau)}$	Pole set	$\alpha'^{(0)}$	$\alpha'^{(I)}$	$\alpha'^{(II)}$
$\frac{3}{2}^+$	CMB	$1.0(1)$	$1.0(1)$	$1.2(2)$
	JüBo	$1.0(1)$	$1.01(4)$	$1.0(1)$
	BnGa	$2.5(2)$	$2.5(2)$	$2.7(3)$
	SAID(SE)	$1.6(1)$	$1.6(1)$	$1.38(8)$
	SAID(ED)	$1.8(1)$	$1.8(1)$	$2.2(2)$
	KH80	$2.7(2)$	$2.9(2)$	$7.6(1)$
	KA84	$1.7(1)$	$1.7(1)$	$2.00(2)$
$\frac{3}{2}^+_{(+)}$	CMB	$0.9(1)$	$0.9(1)$	$1.1(2)$
$\frac{3}{2}^+_{(-)}$	CMB	$1.3(1)$	$1.3(1)$	$1.9(4)$
	Jübo	$0.9(2)$	$0.9(2)$	$1.1(3)$

sibility that $N(1720)$ actually belongs to the parent trajectory. This state is a doublet partner of the $N(1680)$, which we identified in Sec. IV B 1 as a state with physics beyond the compact $3q$ picture. This makes $N(1720)$ a prime candidate to look for additional dynamics, and explains why it might be displaced from the expected pattern and can be missidentified as a member of a daughter trajectory. This state also shows how the inclusion of the width and the patterns in the $(\Im[s_p], J_p)$ allows to better identify if a state is in the leading trajectory or in a subleading one. Again, a better determination of this state would allow further investigation on its nature.

3. $\frac{3}{2}^+$ Regge trajectory

This is the least known parent trajectory, with two well established states –$\Delta(1700)$ and $\Delta(1905)$– and only CMB and JüBo reporting additional resonances. Hence, not much information can be obtained from this trajectory. Comparing all the extractions for $\Delta(1700)$ and $\Delta(1905)$ we see in Figs. 1(b) and 2(b) that $\Re[s_p]$ is reasonably established for both but the width presents large uncertain-

ties. If we consider the CMB and JüBo $7/2^-$ state and CMB $9/2^+$ in Fig. 1(b) a degeneracy breaking is hinted. Hence, we first fit the $\frac{3}{2}^+$ trajectory without considering the degeneracy breaking for all the pole extractions and we also fit $\frac{3}{2}^+_{(+)}$ for JüBo and $\frac{3}{2}^+_{(\pm)}$ for CMB. We provide the parameters in Tables XII–XIV. Because we assume degeneracy in $\frac{3}{2}^+$ fits, the α_0 parameter provides no information. Also, the value of s_t is highly correlated with α_0, so it is not possible to use its value as a way to assess the quality of the extracted parameters. It is clear that degeneracy is a bad approximation to obtain the Regge parameters. Hence, we do not provide consistency checks for this trajectory as they do not provide insight. We note that CMB and JüBo provide a reasonable slope $\alpha' \simeq 1$ GeV^{-2}. JüBo (CMB) provides a consistent slope parameter for $\frac{3}{2}^-_{(-)}$ ($\frac{3}{2}^-_{(+)}$) once degeneracy breaking is considered with $\alpha' \simeq 1$ GeV^{-2}. However, CMB provides a very large slope for $\frac{3}{2}^-_{(-)}$. The overall picture, makes the JüBo extraction of $\frac{3}{2}^+$ the most consistent one, although with very large error bars.

4. $\frac{3}{2}^-$ Regge trajectory

In this trajectory there are three four-star resonances, namely $\Delta(1232)$, $\Delta(1950)$ and $\Delta(2420)$, all of them with even signature. The first two are obtained by all the pole extractions and agree on both mass and width. The higher mass state is found by CMB, SAID(ED), KH80, and KA84 analyses. SAID(ED) and KA84 agree on $\Re[s_p]$, see Fig. 1(b), while KH80 is at odds with their result. If we look into $\Im[s_p]$, Fig. 2(b), SAID(ED) and KH80 disagree, while KA84 extraction overlaps both of them due to its large uncertainty. The CMB extraction of this pole has large uncertainties too and agrees with the other three pole sets within errors.

We perform fits to the odd and even signatures. The fit parameters are reported in Tables XV–XVII. The pa-

Table XV. Parameter α_0 obtained for $\frac{3}{2}^-$ trajectories.

$I^\eta_{(\tau)}$	Pole set	$\alpha_0^{(0)}$	$\alpha_0^{(I)}$	$\alpha_0^{(II)}$
$\frac{3}{2}^-_{(+)}$	JüBo	$-8(8)$	$-11(10)$	$-9(12)$
	SAID(ED)	$13(9)$	$-75(1)$	$34.3(8)$
$\frac{3}{2}^-_{(-)}$	CMB	$0.1(2)$	$-0.1(4)$	$-0.4(5)$
	JüBo	$-0.02(8)$	$-0.1(1)$	$-1.1(6)$
	BnGa	$0.10(1)$	$0.05(1)$	$-0.45(4)$
	SAID(SE)	$0.10(1)$	$0.06(1)$	$-0.39(3)$
	SAID(ED)	$-0.03(3)$	$-0.9(3)$	$-0.43(5)$
	KH80	$0.28(3)$	$0.25(3)$	$0.13(4)$
	KA84	$-0.07(1)$	$-2.1(3)$	$-0.51(3)$

Table XVI. Parameter α' obtained for $\frac{3}{2}^-$ trajectories.

$I^\eta_{(\tau)}$	Pole set	$\alpha'^{(0)}$	$\alpha'^{(I)}$	$\alpha'^{(II)}$
$\frac{3}{2}^-_{(+)}$	JüBo	$4(3)$	$4(3)$	$5(4)$
	SAID(ED)	$-3(2)$	$8.0(2)$	$-4.1(3)$
$\frac{3}{2}^-_{(-)}$	CMB	$0.97(8)$	$1.0(1)$	$1.2(2)$
	JüBo	$1.03(5)$	$1.04(5)$	$1.4(2)$
	BnGa	$0.95(1)$	$0.95(1)$	$1.19(1)$
	SAID(SE)	$0.953(4)$	$0.958(4)$	$1.17(1)$
	SAID(ED)	$1.02(1)$	$1.18(5)$	$1.23(2)$
	KH80	$0.87(1)$	$0.87(1)$	$1.00(2)$
	KA84	$1.04(1)$	$1.36(5)$	$1.28(1)$

rameters for $\frac{3}{2}^-_{(+)}$ are completely at odds with the Regge expectation and the obtained s_t are not physically sensible, *i.e.* $s_t \gg (m_p + m_\pi)^2$. The reasons are obvious if we inspect Fig. 1(b), the position of the $9/2^-$ pole obtained by JüBo and SAID(ED) has a very low $\Re[s_p]$ value given the position of $\Delta(1930)$. Also, in the case of SAID(ED), $\Im[s_p]$ is too large. Hence, the position of this pole is completely unreliable, both in mass and width, as the large uncertainties in the JüBo width hint and no

Table XVII. arameters γ and s_t obtained for $\frac{3}{2}^-$ trajectory.

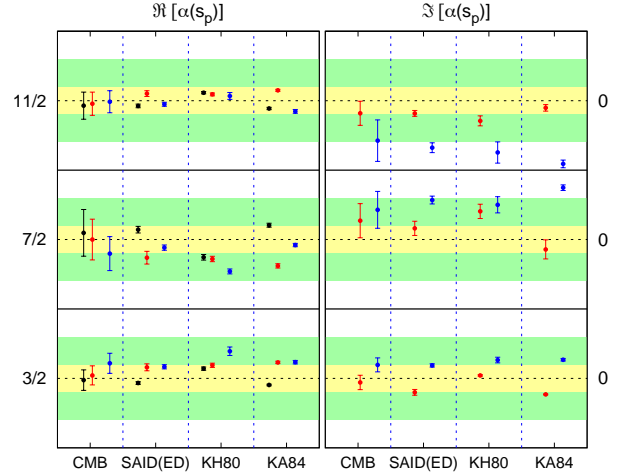| $I^\eta_{(\tau)}$	Pole set	$\gamma^{(I)}$	$\gamma^{(II)}$	$s_t^{(I)}$	$s_t^{(II)}$
$\frac{3}{2}^-_{(+)}$	JüBo	$4(4)$	$4(5)$	$3(3)$	$4(5)$
	SAID(ED)	$28.(2)$	$-8(1)$	$6.6(1)$	$10(2)$
$\frac{3}{2}^-_{(-)}$	CMB	$0.5(1)$	$0.9(2)$	$1.6(3)$	$1.5(1)$
	JüBo	$0.35(7)$	$0.9(3)$	$1.34(9)$	$1.7(2)$
	BnGa	$0.29(1)$	$0.67(2)$	$1.34(1)$	$1.54(1)$
	SAID(SE)	$0.28(1)$	$0.63(2)$	$1.32(1)$	$1.52(1)$
	SAID(ED)	$0.70(9)$	$0.98(3)$	$2.8(3)$	$1.49(1)$
	KH80	$0.39(3)$	$0.80(6)$	$1.39(2)$	$1.40(1)$
	KA84	$1.2(1)$	$1.16(2)$	$3.5(2)$	$1.48(1)$

Figure 4. Consistency checks for $\frac{3}{2}^-_{(-)}$ poles from CMB, SAID(ED), KH80 and KA84 extractions. Notation as in Fig. 3. See Sec. IV B 4 for trajectory definition.

further conclusions can be derived.

Regarding the $\frac{3}{2}^-_{(-)}$ (the Δ trajectory), the effective threshold is at odds with the expected value only for model I in SAID(ED) and KA84 poles. For the rest of pole sets and for model II we obtain reasonable values. The slopes are close to unity as expected and only the α_0 value shows a large variation among models and pole sets. We can compare our Regge parameters to those used in fits to high energy proton-antiproton annihilation, where Δ Regge trajectory $\alpha_\Delta(s) = -0.37 + 0.98\,s$ (s in GeV^2) is one of the main contributions [37]. We note that the slope is close to unity and that the α_0 parameter agrees with the one we obtain for $\frac{3}{2}^-_{(-)}$ using model II. Hence, model II provides the result compatible with the high energy information and our most reliable determination of the parameters. Consequently, as we did in Sec. IV B 1, we can estimate α' from model II values in Table XVI as

$$\alpha'_{\frac{3}{2}^-_{(-)}} = 1.21 \pm 0.15\,\text{GeV}^2.$$

We note that this slope is compatible within errors with the one obtained from the $\frac{1}{2}^+_{(+)}$ trajectory in Sec. IV B 1. The remaining parameters are

$$\alpha_{0,\frac{3}{2}^-_{(-)}} = -0.45 \pm 0.44;$$
$$\gamma_{\frac{3}{2}^-_{(-)}} = 0.86 \pm 0.22;$$
$$s_{t,\frac{3}{2}^+_{(-)}} = 1.52 \pm 0.12\,\text{GeV}^2,$$

with the effective threshold slightly above the expected value of $(m_\pi + m_p)^2 \simeq 1.17$ GeV^2.

Figures 1(b) and 2(b) show a clear linear and square-root-like pattern for the $\frac{3}{2}^-_{(-)}$ trajectory hinting that these states are compact $3q$ structures. However, the consistency check in Fig. 4 provides a sharper image. The

deviations are clear and only CMB provides an approximate agreement between theory and data, mostly due to the large uncertainties. Considering that CMB overlaps with the pole extractions by other analyses, its deviation from the trajectory models in Eq. (5) signals the effects of beyond compact $3q$ physics, even for the well-studied $\Delta(1232)$ state. The $\frac{3}{2}^-_{(-)}$ poles are known well enough to be sensitive to these beyond compact $3q$ effects.

V.   SUMMARY AND CONCLUSIONS

We have studied the structure of the N^* and Δ^* spectra from the perspective of Regge and complex angular momentum theory following the work done for the strange baryon sector in [6]. We have considered seven pole extractions [30–36]. In our analysis we have taken into account the fact that poles are complex quantities, and we go beyond the standard studies that focus only in the Chew-Frautschi plot $(\Re[s_p], J_p)$ and linear trajectory fits to said plot. In doing so, we also study the $(\Im[s_p], J_p)$ plots introduced in [6]. We find many discrepancies among the pole extractions, in particular for the widths, but a clear pattern, similar to the one in the strange sector, appears where the Chew-Frautschi plots follow the well-known approximate linear behavior, while the $(\Im[s_p], J_p)$ plots show a square-root-like behavior.

Our working hypothesis has been that the square-root-like behavior appreciated in Fig. 2 is due to the contribution of the phase space to the scattering amplitude [51], which is proportional to the momentum $q \sim \sqrt{s - s_t}$. The phase space is the main contribution to how deep in the complex plane the poles are. Major deviations from that pattern would signal an important component of beyond compact $3q$ physics, *i.e.* additional QCD dynamics. Under this hypothesis, a state that presents a linear trajectory in the Chew-Frautschi plot *and* a square-root-like behavior would be mostly a compact $3q$ state. Besides the qualitative analysis of the plots, we performed a quantitative one, modeling the Regge trajectories, fitting the poles and cross checking the consistency of the results. The results support the qualitative conclusions but also signal sizable physics beyond the compact $3q$ picture for the $N(1680)$, the $N(1720)$ and some of the members of the $\frac{3}{2}^-_{(-)}$ trajectory. The last poles are known well enough that our analysis is sensitive to beyond compact $3q$ effects.

We find that exchange degeneracy is very clearly broken in the nonstrange sector, contrary to the strange sector. This degeneracy breaking shows the importance of exchange forces in the determination of the low-lying nonstrange baryon spectrum. We also find that the $\frac{1}{2}^-$ and $\frac{3}{2}^+$ trajectories are poorly known and Regge phenomenology cannot provide insight on the internal structure of the baryons. However, Regge phenomenology serves as a guide for resonance searches. Particularly, as a way to explore if the fits to the experimental data are improved by including resonances close to the expected positions in both Chew-Frautschi and $(\Im[s_p], J_p)$ plots.

The parameters of the $\frac{1}{2}^+_{(+)}$ (nucleon) and $\frac{3}{2}^-_{(-)}$ (Δ) Regge trajectories can be well established from the poles. We estimate $\alpha' = 0.99 \pm 0.12$ GeV^{-2} for the nucleon trajectory and $\alpha' = 1.21 \pm 0.15$ GeV^{-2} for the Δ. We note that both slopes are compatible within errors. This range is consistent with α' obtained from fits to the Chew-Frautschi plots, with what is predicted by constituent quark models and with fits to high energy proton-antiproton annihilation.

[1] P. D. B. Collins, *An Introduction to Regge Theory and High-Energy Physics*, Cambridge Monographs on Mathematical Physics (Cambridge Univ. Press, Cambridge, UK, 2009).

[2] V. N. Gribov, *The theory of complex angular momenta: Gribov lectures on theoretical physics*, Cambridge Monographs on Mathematical Physics (Cambridge University Press, 2007).

[3] V. N. Gribov, *Strong interactions of hadrons at high energies: Gribov lectures on Theoretical Physics*, edited by Y. L. Dokshitzer and J. Nyiri (Cambridge University Press, 2012).

[4] J. T. Londergan, J. Nebreda, J. R. Peláez, and A. Szczepaniak, Phys. Lett. **B729**, 9 (2014), arXiv:1311.7552 [hep-ph].

[5] J. A. Carrasco, J. Nebreda, J. R. Peláez, and A. P. Szczepaniak, Phys. Lett. **B749**, 399 (2015), arXiv:1504.03248 [hep-ph].

[6] C. Fernández-Ramírez, I. V. Danilkin, V. Mathieu, and A. P. Szczepaniak, Phys. Rev. **D93**, 074015 (2016), arXiv:1512.03136 [hep-ph].

[7] J. R. Peláez and A. Rodas, Eur. Phys. J. **C77**, 431 (2017),

arXiv:1703.07661 [hep-ph].

[8] G. F. Chew and S. C. Frautschi, Phys. Rev. Lett. **8**, 41 (1962).

[9] J. Greensite, Lect. Notes Phys. **821**, 1 (2011).

[10] G. C. Rossi and G. Veneziano, Nucl. Phys. **B123**, 507 (1977).

[11] L. Montanet, G. C. Rossi, and G. Veneziano, Phys. Rept. **63**, 149 (1980).

[12] V. N. Gribov, Sov. Phys. JETP **15**, 873 (1962), [Nucl. Phys.40,107(1963)].

[13] R. Fiore, L. L. Jenkovszky, V. Magas, F. Paccanoni, and A. Papa, Eur. Phys. J. **A10**, 217 (2001), arXiv:hep-ph/0011035 [hep-ph].

[14] R. Fiore, L. L. Jenkovszky, F. Paccanoni, and A. Prokudin, Phys. Rev. **D70**, 054003 (2004), arXiv:hep-ph/0404021 [hep-ph].

[15] H. Nakkagawa, K. Yamawaki, and S. Machida, Prog. Theor. Phys. **48**, 939 (1972).

[16] R. Bijker, F. Iachello, and A. Leviatan, Annals Phys. **236**, 69 (1994), arXiv:nucl-th/9402012 [nucl-th].

[17] R. Bijker, F. Iachello, and A. Leviatan, Annals Phys. **284**, 89 (2000), arXiv:nucl-th/0004034 [nucl-th].

[18] E. Ortiz-Pacheco, R. Bijker, and C. Fernández-Ramírez, (2018), arXiv:1808.10512 [nucl-th].

[19] S. Capstick and N. Isgur, Phys. Rev. **D34**, 2809 (1986).

[20] U. Loring, B. C. Metsch, and H. R. Petry, Eur. Phys. J. **A10**, 395 (2001), arXiv:hep-ph/0103289 [hep-ph].

[21] A. Inopin and G. S. Sharov, Phys. Rev. **D63**, 054023 (2001), arXiv:hep-ph/9905499 [hep-ph].

[22] A. Tang and J. W. Norbury, Phys. Rev. **D62**, 016006 (2000), arXiv:hep-ph/0004078 [hep-ph].

[23] S. Godfrey and N. Isgur, Phys. Rev. **D32**, 189 (1985).

[24] M. Koll, R. Ricken, D. Merten, B. C. Metsch, and H. R. Petry, Eur. Phys. J. **A9**, 73 (2000), arXiv:hep-ph/0008220 [hep-ph].

[25] D. Ebert, R. N. Faustov, and V. O. Galkin, Phys. Rev. **D79**, 114029 (2009), arXiv:0903.5183 [hep-ph].

[26] N. Isgur and J. E. Paton, Phys. Rev. **D31**, 2910 (1985).

[27] M. G. Olsson, S. Veseli, and K. Williams, Phys. Rev. **D53**, 4006 (1996), arXiv:hep-ph/9501323 [hep-ph].

[28] C. Semay, F. Buisseret, N. Matagne, and F. Stancu, Phys. Rev. **D75**, 096001 (2007), arXiv:hep-ph/0702075 [hep-ph].

[29] M. Tanabashi *et al.* (Particle Data Group), Phys. Rev. **D98**, 030001 (2018).

[30] R. E. Cutkosky, C. P. Forsyth, R. E. Hendrick, and R. L. Kelly, Phys. Rev. **D20**, 2839 (1979).

[31] R. E. Cutkosky, C. P. Forsyth, J. B. Babcock, R. L. Kelly, and R. E. Hendrick, in *Baryon 1980. Proceedings, 4th International Conference on Baryon Resonances, Toronto, Canada, July 14-16, 1980* (1980) p. 19.

[32] D. Rönchen, M. Döring, and U. G. Meißner, Eur. Phys. J. **A54**, 110 (2018), arXiv:1801.10458 [nucl-th].

[33] A. V. Anisovich, R. Beck, E. Klempt, V. A. Nikonov, A. V. Sarantsev, and U. Thoma, Eur. Phys. J. **A48**, 15 (2012), arXiv:1112.4937 [hep-ph].

[34] V. Sokhoyan *et al.* (CBELSA/TAPS), Eur. Phys. J. **A51**, 95 (2015), [Erratum: Eur. Phys. J.A51,187(2015)], arXiv:1507.02488 [nucl-ex].

[35] A. Švarc, M. Hadžimehmedović, H. Osmanović, J. Stahov, and R. L. Workman, Phys. Rev. **C91**, 015207 (2015), arXiv:1405.6474 [nucl-th].

[36] A. Švarc, M. Hadžimehmedović, R. Omerović, H. Osmanović, and J. Stahov, Phys. Rev. **C89**, 045205 (2014),

arXiv:1401.1947 [nucl-th].

[37] J. Van de Wiele and S. Ong, Eur. Phys. J. **A46**, 291 (2010), arXiv:1004.2152 [nucl-th].

[38] J. Nys, V. Mathieu, C. Fernández-Ramírez, A. N. Hiller Blin, A. Jackura, M. Mikhasenko, A. Pilloni, A. P. Szczepaniak, G. Fox, and J. Ryckebusch (JPAC), Phys. Rev. **D95**, 034014 (2017), arXiv:1611.04658 [hep-ph].

[39] V. Mathieu, J. Nys, A. Pilloni, C. Fernández-Ramírez, A. Jackura, M. Mikhasenko, V. Pauk, A. P. Szczepaniak, and G. Fox, EPL **122**, 41001 (2018), arXiv:1708.07779 [hep-ph].

[40] V. Mathieu, J. Nys, C. Fernández-Ramírez, A. N. Hiller Blin, A. Jackura, A. Pilloni, A. P. Szczepaniak, and G. Fox (JPAC), Phys. Rev. **D98**, 014041 (2018), arXiv:1806.08414 [hep-ph].

[41] R. L. Workman, R. A. Arndt, W. J. Briscoe, M. W. Paris, and I. I. Strakovsky, Phys. Rev. **C86**, 035202 (2012), arXiv:1204.2277 [hep-ph].

[42] G. Höhler, *Pion Nucleon Scattering. Part 2: Methods and Results of Phenomenological Analyses*, edited by H. Schopper, Landolt-Bornstein (Springer-Verlag Berlin Heidelberg, 1983).

[43] R. Koch, Z. Phys. **C29**, 597 (1985).

[44] R. Koch, Nucl. Phys. **A448**, 707 (1986).

[45] G. Höhler, *Proceedings of the 5th International Symposium on Meson-Nucleon Physics and the Structure of the Nucleon, Vol. II, Boulder, Colorado, September 6-10, 1993*, πN Newsletter **9**, 1 (1993).

[46] M. Shrestha and D. M. Manley, Phys. Rev. **C86**, 055203 (2012), arXiv:1208.2710 [hep-ph].

[47] T. P. Vrana, S. A. Dytman, and T. S. H. Lee, Phys. Rept. **328**, 181 (2000), arXiv:nucl-th/9910012 [nucl-th].

[48] V. Shklyar, H. Lenske, and U. Mosel, Phys. Rev. **C87**, 015201 (2013), arXiv:1206.5414 [nucl-th].

[49] H. Kamano, S. X. Nakamura, T. S. H. Lee, and T. Sato, Phys. Rev. **C88**, 035209 (2013), arXiv:1305.4351 [nucl-th].

[50] M. Batinic, S. Ceci, A. Svarc, and B. Zauner, Phys. Rev. **C82**, 038203 (2010).

[51] G. F. Chew and S. Mandelstam, Phys. Rev. **119**, 467 (1960).

[52] C. B. Chiu, Ann. Rev. Nucl. Part. Sci. **22**, 255 (1972).

[53] S. Mandelstam, Phys. Rev. **166**, 1539 (1968).

[54] G. Veneziano, Nuovo Cim. **A57**, 190 (1968).

[55] A. P. Szczepaniak and M. R. Pennington, Phys. Lett. **B737**, 283 (2014), arXiv:1403.5782 [hep-ph].

[56] A. I. Bugrij, G. Cohen-Tannoudji, L. L. Jenkovszky, and N. A. Kobylinsky, Fortsch. Phys. **21**, 427 (1973).

[57] L. L. Jenkovszky, Sov. J. Nucl. Phys. **21**, 334 (1975), [Yad. Fiz.21,645(1975)].

[58] M. Shi, I. V. Danilkin, C. Fernández-Ramírez, V. Mathieu, M. R. Pennington, D. Schott, and A. P. Szczepaniak, Phys. Rev. **D91**, 034007 (2015), arXiv:1411.6237 [hep-ph].

[59] W. H. Press, S. A. Teukolsky, W. T. Vetterling, and B. P. Flannery, *Numerical Recipes 3rd Edition: The Art of Scientific Computing*, 3rd ed. (Cambridge University Press, New York, NY, USA, 2007).

[60] B. Efron and R. Tibshirani, *An Introduction to the Bootstrap*, Chapman & Hall/CRC Monographs on Statistics & Applied Probability (Taylor & Francis, 1994).

[61] J. Landay, M. Döring, C. Fernández-Ramírez, B. Hu, and R. Molina, Phys. Rev. **C95**, 015203 (2017), arXiv:1610.07547 [nucl-th].

[62] D. Molina, M. De Sanctis, and C. Fernández-Ramírez, Phys. Rev. **D95**, 094021 (2017), arXiv:1703.08097 [hep-ph].

[63] C. Fernández-Ramírez and A. Relaño, Phys. Rev. Lett. **98**, 062001 (2007), arXiv:hep-ph/0701111 [hep-ph].

[64] S. W. MacDowell, Phys. Rev. **116**, 774 (1959).